

Experimental research on seismic behavior of steel reinforced high-strength concrete short columns

Weiqing Zhu^{*1}, Jinqing Jia^{2a} and Janguang Zhang^{3b}

¹School of Highway, Chang'an University, Xi'an 710064, P.R. China

²Faculty of Infrastructure Engineering, Dalian University of Technology, Dalian 116024, P.R. China

³Bureau of Traffic Construction Engineering Quality Supervision of Inner Mongolia Autonomous Region, Hohhot 010010, P.R. China

(Received June 29, 2017, Revised August 29, 2017, Accepted September 03, 2017)

Abstract. This experimental research presents the seismic performance of steel reinforced high-strength concrete (SRHC) short columns. Eleven SRHC column specimens were tested under simulated earthquake loading conditions, including six short column specimens and five normal column specimens. The parameters studied included the axial load level, stirrup details and shear span ratio. The failure modes, critical region length, energy dissipation capacity and deformation capacity, stiffness and strength degradation and shear displacement of SRHC short columns were analyzed in detail. The effects of the parameters on seismic performance were discussed. The test results showed that SRHC short columns exhibited shear-flexure failure characteristics. The critical region length of SRHC short columns could be taken as the whole column height, regardless of axial load level. In comparison to SRHC normal columns, SRHC short columns had weaker energy dissipation capacity and deformation capacity, and experienced faster stiffness degradation and strength degradation. The decrease in energy dissipation and deformation capacity due to the decreasing shear span ratio was more serious when the axial load level was higher. However, SRHC short columns confined by multiple stirrups might possess good seismic behavior with enough deformation capacity (ultimate drift ratio $\geq 2.5\%$), even though a relative large axial load ratio ($= 0.38$) and relative small structural steel ratio ($= 3.58\%$) were used, and were suitable to be used in tall buildings in earthquake regions.

Keywords: steel reinforced concrete; high-strength concrete; composite column; short column; seismic performance; shear span ratio

1. Introduction

Tall buildings are becoming common in urban areas. Larger column sizes are usually required to carry the huge axial loads in buildings. However, minimizing column sizes is desirable for increasing floor space. So, High-strength concrete (HSC) columns, which possess increased stiffness and strength, and carry larger loads, have the potential to be widely used in tall buildings. From the safety point of view, ductility should be treated as critical as strength for columns in seismic regions. However, HSC columns are much more brittle than normal-strength concrete (NSC) columns (Bai and Au 2013, Hong *et al.* 2006, Lam *et al.* 2009, Légeron and Paultre 2000). To improve the ductility behavior of HSC columns, many efforts have been made, such as, confining the HSC by stirrups or helices (Hadi 2005, Ho *et al.* 2010, Paultre *et al.* 2001), FRP or CRFP laminates (Hassan *et al.* 2017, Pham and Hadi 2014, Wang *et al.* 2017), or steel tube (Wang and Liew 2016), reinforcing the concrete by steel fiber (Afroughsabet and Ozbakkaloglu

2015), and so on.

Steel reinforced concrete (SRC, one type of composite structure sections) columns exhibit large bearing capacity, high stiffness levels, as well as excellent ductility due to the usage of structural steel (Chen *et al.* 2016, Chen and Lin 2006, Ellobody and Young 2011, Fang *et al.* 2015, Ma *et al.* 2013, 2016, Naito *et al.* 2011, Xue *et al.* 2012). Therefore, steel reinforced high-strength concrete (SRHC) columns should have high levels of stiffness and strength as well as good seismic ductility because HSC and SRC are adopted simultaneously. Some useful researches on SRHC columns have been conducted in the past several decades. Most of the studies have focused on the ductility of SRHC columns because of the brittleness of HSC. A fiber section analysis by El-Tawil and Deierlein (1999) found that the structural steel can resist a percentage of the axial load and moment, and can provide confinement to concrete between its flanges. However, it also found that SRHC columns had low curvature ductility if they were subjected to large axial loads, and relied on a higher degree of stirrups to offer a certain level of ductility relative to SRC columns with NSC. Subsequently, experimental studies by Jia *et al.* (2006) and Zheng *et al.* (2012) found that carrying capacity and ductility factor are greater for SRHC columns compared to those for the corresponding HSC columns. However, those studies showed that the tested SRHC columns might have unsatisfactory seismic behavior, particularly for large axial loads and small shear span ratios. Those experimental

*Corresponding author, Assistant Professor,

E-mail: zhuweiqing87@126.com

^a Ph.D.,

E-mail: keyknown@163.net

^b Ph.D.,

E-mail: zjg829@163.com

Table 1 Concrete mix designs (per cubic meter)

Cement (kg)	Fly ash (kg)	Silica fume (kg)	Coarse aggregate (kg)	Sand (kg)	Water-reducing admixture (%)	Retarder (0.01%)	W/B ratio
420	120	60	1155	495	1.5	4.5	0.23

Table 2 Mechanical properties of steel

Reinforcement	Diameter (mm)	Cross area A_s (mm ²)	Young's modulus E_s (MPa)	Yielding strength f_y (MPa)	Ultimate strength f_u (MPa)
$\Phi 10$	10	78.5	205×10^3	414	597
$\Phi 6$	6	28.3	201×10^3	499	718
Structural steel	Size $h \times b \times t_w \times t_f$ (mm)	Cross area A_{ss} (mm ²)	Young's modulus E_s (MPa)	Yielding strength f_{ys} (MPa)	Ultimate strength f_{us} (MPa)
I10	100×68×4.5×7.6	1430	207×103	254	368

results showed that the unsatisfactory ductility could be due to the rectangular stirrups and I-shaped structural steel, which provide weak confinement to the HSC in columns. So, experimental studies on the axial load performance of SRHC short columns were carried out by Zhu *et al.* (2014).

It was found that SRHC columns with multiple stirrups had significantly better ductility factors than columns with rectangular stirrups, even when the volumetric ratios of the stirrups were the same. Based on the axial load test, twenty-one SRHC normal columns with a shear span ratio of $\lambda = 3.0$ were tested under pseudo static loading conditions (Zhu *et al.* 2016). The research concluded that SRHC normal columns with multiple stirrups and commonly used structural steel ratios exhibited excellent seismic behavior with sufficient energy dissipation and deformation capacity.

The benefits of structural steel are more obvious when confinement of stirrups is stronger. So, multiple stirrups should be used in SRHC columns in order to provide full play for the structural steel. At the same time, structural steel heightens the positive effects of stirrups. Therefore, we now understand the reason for the unsatisfactory seismic behavior of SRHC columns tested by Jia *et al.* (2006) and Zheng *et al.* (2012), and SRHC columns provides another practical solution to the above mentioned problem.

“Short” columns are defined as columns with shear span ratios of $\lambda = M/Vh = L/h \leq 2.5$. M and V are the moment and shear force acting at the end cross section, respectively, L is the length from the point of contra-flexure to the end cross section, and h is the depth of the cross section (Moretti and Tassios 2006). Short columns are common in the lower floors of tall buildings because they are subjected to huge axial loads. RC short columns subjected to cyclic lateral displacement usually manifest a particular brittle behavior (Moretti and Tassios 2007, Xiao and Zhang 2006). Most importantly, SRHC short columns with $\lambda \leq 2.5$ have not yet been demonstrated to have good seismic behavior. For example, SRHC short columns tested by Jia *et al.* (2006) with a shear span ratio of $\lambda = 2.0$, axial load level of $P/P_0 = 0.35$, rectangular stirrup volumetric ratio of $\rho_{sv} = 1.2\text{--}2.2\%$, and structural steel ratio of $\rho_{ss} = 3.7\%$, had small ultimate drift ratios ($\theta_u \leq 1.5\%$) and displacement ductility factors ($\mu_\Delta \leq 2.5$), and exhibited a shear failure mode. Therefore,

based on the work on SRHC normal columns (Zhu *et al.* 2016), this paper conducted a simulated earthquake loading test on SRHC short columns to study the seismic performance of SRHC short columns, and to prove that SRHC short columns possess enough deformation capacity, and are suitable to be used in earthquake regions.

2. Experimental program

2.1 Material properties

High-strength concrete was adopted in this test. HSC with excellent workability was mixed according to the proportions listed in Table 1. The concrete mixture was made with ordinary Portland cement, fly ash, silica fume, coarse aggregate and sand. To improve the workability, high-range water-reducing admixture and retarder were added. The $150 \times 150 \times 300$ mm prism specimens for use in measuring the concrete strength and Young's modulus were cast. The prism specimens were cured with column specimens in the same outdoor conditions. The concrete material test was carried out immediately before the simulated earthquake loading test.

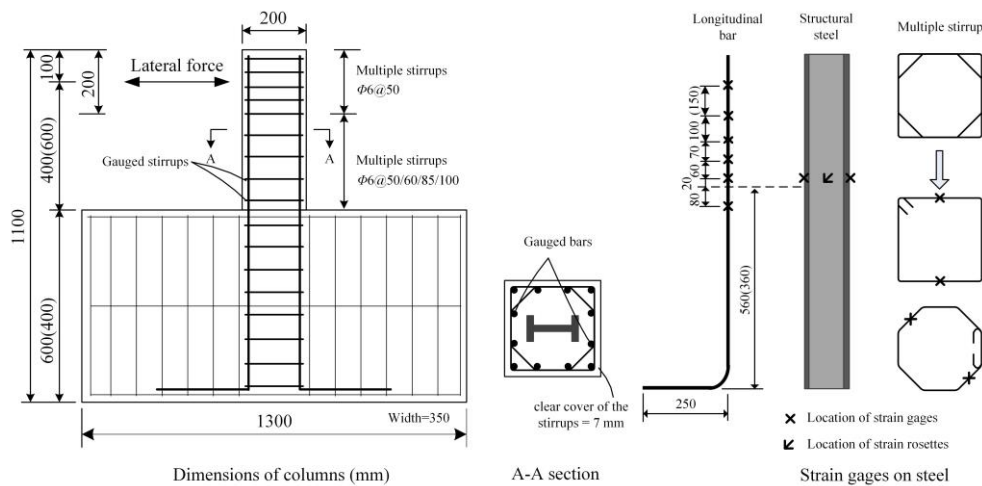
Hot-rolled deformed steel bars with diameters of 10 and 6 mm were used for longitudinal reinforcements and transverse stirrups, respectively. No. 10 I-shaped (I10) steel was used for structural steel in the column specimens. The material properties of steel and concrete are summarized in Tables 2 and 3, respectively.

2.2 Test specimens

A total of eleven SRHC column specimens were reported, including six short column specimens and five normal column specimens as shown in Table 3. The six short column specimens were fabricated and tested in this paper. The five normal column specimens tested in the companion paper (Zhu *et al.* 2016) were also collected and re-analyzed for comparison. The specimen details of both the short and normal column specimens are presented in Fig. 1. The columns were fabricated with a 200×200 mm cross

Table 3 Design parameters of specimens

Specimen	f_c (MPa)	E_c (MPa)	Axial load level			Transverse reinforcement			shear span ratio
			P (kN)	$n = P / A_g f_c$	$n' = P / P_0$	Type	Spacing (mm)	ρ_{sv} (%)	
1-A-N2-M50	107.3	488 00	1600	0.38	0.34	Multiple	50	2.00	2.0
2-A-N2-M60	107.3	488 00	1600	0.38	0.34	Multiple	60	1.67	2.0
3-A-N1-M85	107.3	488 00	1050	0.25	0.22	Multiple	85	1.18	2.0
4-A-N2-M85	104.0	472 00	1600	0.38	0.34	Multiple	85	1.18	2.0
5-A-N1-M100	104.0	472 00	1050	0.25	0.22	Multiple	100	1.00	2.0
6-A-N2-M100	104.0	472 00	1600	0.38	0.34	Multiple	100	1.00 <td 2.0	
7-B-N2-M50	99.8	487 00	1600	0.38	0.34	Multiple	50	2.00	3.0
8-B-N2-M60	107.0	493 00	1600	0.38	0.34	Multiple	60	1.67	3.0
9-B-N2-M85	103.7	468 00	1600	0.38	0.34	Multiple	85	1.18	3.0
10-B-N1-M100	105.4	470 00	1050	0.25	0.22	Multiple	100	1.00	3.0
11-B-N2-M100	109.5	491 00	1600	0.38	0.34	Multiple	100	1.00	3.0



Note: Dimensions marked in brackets are for normal column specimens with $\lambda = 3.0$

Fig. 1 SRHC short and normal column specimen details

section, and with a height of 400 mm (or 600 mm) from the position of the lateral force to the RC stub footing. Each short column (or normal column) had a shear span ratio of $\lambda = 400 \text{ mm}/200 \text{ mm} = 2.0$ (or $\lambda = 600 \text{ mm}/200 \text{ mm} = 3.0$). The RC stub footing cast with the column had a cross section of $350 \times 600 \text{ mm}$ (or $350 \times 400 \text{ mm}$), and was heavily reinforced. So, the RC stub footing represented a rigid member such as a beam-column joint or stiff foundation. The total height (1100 mm) and horizontal loading point (1000 mm above the floor) of the two types of specimens were the same, so the test frame did not need to be re-adjusted.

All the columns were reinforced with twelve $\Phi 10 \text{ mm}$ longitudinal reinforcements with a reinforcement ratio of $\rho_l = 2.36\%$, and an I10 structural steel with a structural steel ratio of $\rho_{ss} = 3.58\%$. Both the longitudinal bars and structural steel were fully anchored into the RC stub, as shown in Fig. 1. $\Phi 6 \text{ mm}$ bars were used as transverse reinforcements. To prevent concrete crushing during the test, multiple stirrups with 50 mm spacing were adopted in the

top 200 mm of the columns. The details for all columns were determined by the flexural failure conditions before shear failure.

2.3 Test variables

The companion work (Zhu *et al.* 2016) conducted a detailed research on the seismic behavior of SRHC normal columns with a shear to span ratio of $\lambda = 3.0$. Based on the conclusions of that paper, the test series in this study was designed to study the influence of the following parameters on the seismic behavior of SRHC short columns.

- Axial load level. The axial load level is defined by the axial load ratio (n), i.e., the ratio of the applied axial load (P) to the gross concrete axial load capacity of the column ($A_g f_c$). It can also be defined by the ratio of applied axial load to the nominal axial load capacity ($n' = P/P_0$). The axial load applying in the column was maintained constant at 1050 or 1600 kN. To figure out the axial load level, compressive concrete strength was

taken as the average value of all columns ($f_c = 105.4$ MPa). Therefore, the two axial loads were corresponding to axial load ratios of $n = 0.25$ or 0.38 . The value of $n = 0.25$ (i.e., $n' = 0.22$) approximately corresponded to a balanced failure of a concrete column section. The latter was considered as a high level of axial load. At the same time, the latter was usually taken as the limit value specified for SRC with NSC by Chinese specification for SRC composite structures JGJ138 (2001).

- **Stirrup details.** Previous studies (Zhu *et al.* 2014, Zhu *et al.* 2016) showed that stirrups have a significant positive influence on the ductility of SRHC columns. Stirrup type is more effective than stirrup spacing to enhance the ductility, meaning that the influence efficiency of stirrups on ductility depends on stirrup type to a great extent. Therefore, multiple stirrups were adopted in all column specimens. Spacings of 50, 60, 85, and 100 mm were studied, and provided volumetric ratios of $\rho_{sv} = 2.00, 1.67, 1.18, \text{ and } 1.00\%$, respectively. The spacings of 85 and 100 mm were corresponding to the minimum values required in JGJ138 (2001), respectively. Other stirrup spacings were to get better ductile behavior.

- **Shear span ratio.** The six SRHC short column specimens had a shear span ratio of $\lambda = 2.0$. For comparison, other specimens (considered to behave as normal long columns) had a shear span ratio of $\lambda = 3.0$.

A string of characters was used to label the column specimens, beginning with the specimen number (1, 2 . . .) followed by the shear span ratio (A or B for $\lambda = 2.0$ and 3.0 , respectively), the axial load ratio (N1 or N2 for $n = 0.25$ and 0.38 , respectively), and the stirrup type (M) and spacing in millimeters (40, 50, 60, or 85). To facilitate the comparative study, the normal column specimens collected from the companion work (Zhu *et al.* 2016) were re-labeled according to the above rule in this paper.

2.4 Test setup and instrumentation

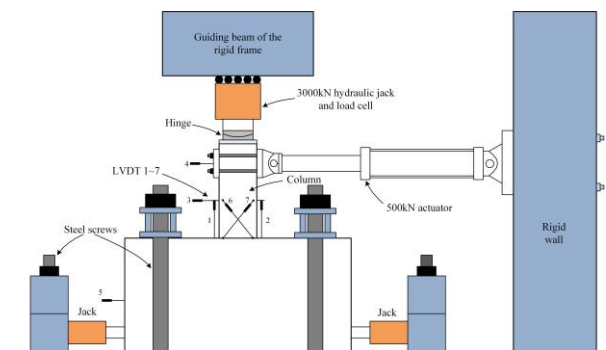
The specimens were tested in the vertical position and subjected to cyclic lateral forces and constant axial loads using a specially designed test rig. Fig. 2 shows a drawing and photograph of a short column specimen in the test apparatus. The stub footing was fixed to the laboratory stiff floor by using of screws and jacks, to prevent sliding and overturning of specimens. Axial and horizontal loads were applied using the 3000 kN hydraulic jack and the 500 kN tension/compression actuator, respectively.

The specimens were instrumented to monitor both global and local response quantities. Three types of measuring devices were used during testing: load cells, strain gauges, and linear variable displacement transducers (LVDTs). For global response quantities, the axial compression in the column was measured by the load cell located between the hydraulic jack and the column. The horizontal load was measured by the actuator load cell. And the lateral tip displacement was measured by using an LVDT with a range of 100 mm. For local response quantities, several strain gages were arranged on selected

longitudinal reinforcements to monitor the strain distribution in the bars. Two strain gages were placed on flange and one (0 for normal column specimens) strain rosette was arranged on the web of the structural steel. The remaining eight strain gages were used to monitor stirrup strains at selected positions. At the same time, several additional LVDTs were arranged to measure the relative deformation along the columns. The arrangements of all above mentioned instrumentations of short column specimens are shown in Figs. 1 and 2. Test setup and instrumentation details of normal column specimens can be found in the companion paper.

2.5 Test procedure

The direction of lateral loading is defined as follows: the “push” direction relates to column deflections away from the rigid wall, while the “pull” direction relates to deflections toward the rigid wall. During the tests, the axial load was kept at approximately constant levels. The horizontal force was cycled with a scheduled displacement-control mode. The first two cycles with peak drift ratios of $\theta = 0.25$ and 0.5% were initially applied. Cycles with peak drift ratios of $\theta = 1.0, 1.5, 2.0, \text{ and } 2.5\%$ were then applied, and these cycles were repeated three times. The scheduled cyclic loading protocol is shown in Fig. 3. It should be note that, the tip displacement of short column specimens was different from that of normal columns specimens if the drift ratio was the same. The test ended if the specimen was unable to carry the axial load or the lateral force dropped to less than 80% peak value.



(a) Schematic diagram



(b) Photograph of test setup and testing frame

Fig. 2 Test setup

Table 4 Summary of test results

Specimen	I_e	K_0 (kN/m)	F_{sp} (kN)	F_p (kN)	E_{sum} (kN·m)	Δ_y (mm)	Δ_u (mm)	μ_Δ	θ_u (%)	L_p (mm)	L_c (mm)	L_{bl} (mm)	L_{bs} (mm)	Failure mode
1-A-N2-M50	0.033	106100	287.3	296.8	28.6	2.2	12.0	5.5	3.0	300	300	220	200	S-F
2-A-N2-M60	0.025	102200	294.0	305.5	30.3	2.9	11.0	3.8	2.7	350	350	200	150	S-F
3-A-N1-M85	0.015	80900	301.5	340.1	35.2	4.0	13.1	3.3	3.3	330	330	240	120	S-F
4-A-N2-M85	0.015	102500	309.9	309.9	19.4	2.4	9.3	3.9	2.3	350	350	150	190	S-F
5-A-N1-M100	0.011	80600	292.8	295.4	25.4	3.4	12.4	3.6	3.1	320	320	180	160	S-F
6-A-N2-M100	0.011	110900	301.2	309.2	10.9	2.4	8.4	3.5	2.1	350	350	160	220	S-F
7-B-N2-M50	0.033	48600	200.3	274.2	66.1	3.7	21.0	5.7	3.5	350	350	180	160	F
8-B-N2-M60	0.025	48000	224.7	289.0	48.3	5.8	21.0	3.6	3.5	410	410	260	200	F
9-B-N2-M85	0.015	47900	208.9	208.9	22.3	4.6	15.0	3.3	2.5	400	400	220	190	F
10-B-N1-M100	0.011	47500	206.6	228.6	32.7	5.3	18.0	3.4	3.0	300	300	200	170	F
11-B-N2-M100	0.011	49300	221.5	221.5	21.9	4.8	15.0	3.1	2.5	430	430	200	200	F

Note: S-F represents shear-flexure failure, and F represents flexure failure

3. General observations and failure modes

Two different failure modes could be observed, depending on the shear span ratio of specimens, as shown in Table 4. Normal columns ($\lambda = 3$) exhibited flexure-controlled failure, while short columns ($\lambda = 2$) exhibited shear-flexure failure characteristics. The damage sequence was similar for columns with the same failure modes, but different for columns with different failure modes. For comparison, the most notable observations in the sequence of first occurrence (such as cover concrete spalling) are recorded and marked in the corresponding cycles of the measured lateral force versus tip displacement hysteretic curves, as shown in Fig. 4. The damage states of short and normal columns are described in the following sections.

3.1 Short columns

Fig. 5 shows the propagation of damage at different steps in two short column specimens subjected to different axial load levels.

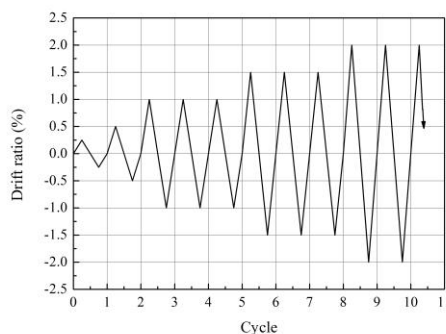


Fig. 3 Cyclic loading protocol

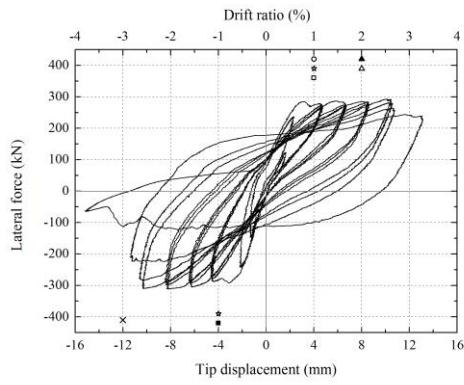
3.1.1 Cover spalling and concrete cracking

When drifts were not greater than 0.5%, all short columns behaved elastically, without concrete cracking or cover concrete spalling. Initial cover spalling at column corners and faces perpendicular to the lateral force (Fig. 5) occurred suddenly with a loud noise, at the first cycle of drift 1.0% or 1.5% depending on the axial load level. That is, it happened at a drift of 1.0% if $n = 0.38$, and 1.5% if $n = 0.25$. The first cracking occurred (inclined crack) at a drift ratio of 1.0% for all short columns. By increasing the lateral displacement, new cracks formed and old cracks extended.

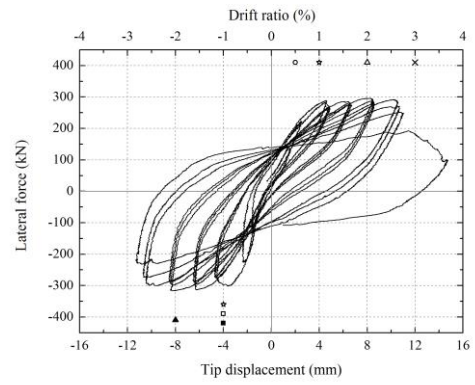
The inclined cracks propagated to the whole column height. At the same time, several main diagonal cracks formed gradually at each column face parallel to the lateral force. Cover spalling gradually spread over the column surfaces, accompanied by concrete cracking. For columns with lower axial load levels and more stirrups, the region of cover spalling was smaller, crack widths were smaller, and cracking occurred in a more diffuse manner. At drifts after the yielding of the stirrups and structural web, core concrete just confined by stirrups [i.e., partially confined concrete (El-Tawil and Deierlein 1999)] also crushed more or less. After the column failed, it was found that the cracks did not penetrate into the un-crushed core concrete (Fig. 5).

3.1.2 Bar and structural steel flange yielding and buckling

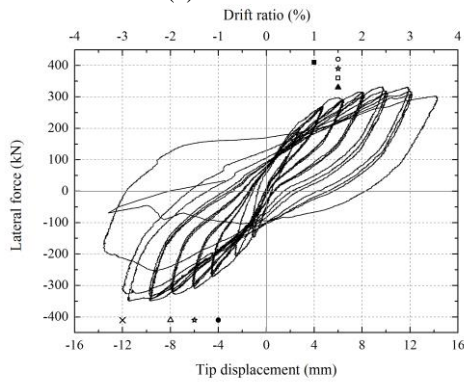
The yielding of longitudinal bars and structure steel flange resulted from the axial load and bending moment; therefore, yielding happened at different times for different axial load levels. The initial yielding of bars and structural steel flanges is shown in Fig. 4. Once the cover concrete spalled off, the stirrups and longitudinal reinforcements were exposed. Then, longitudinal bar buckling could be observed, as shown in Fig. 5. The buckled bar region covered several stirrup spacings, which mainly depended on the axial load level.



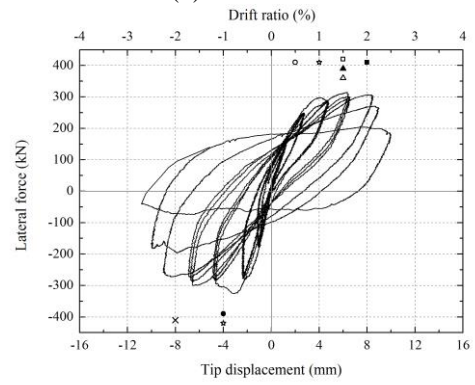
(a) 1-A-N2-M50



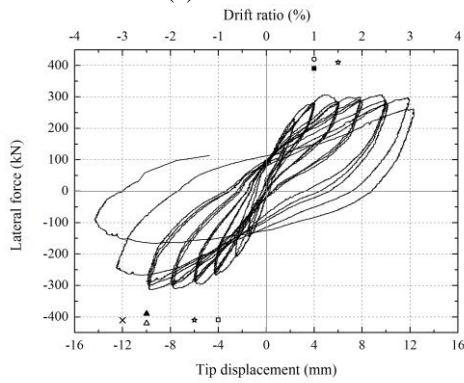
(b) 2-A-N2-M60



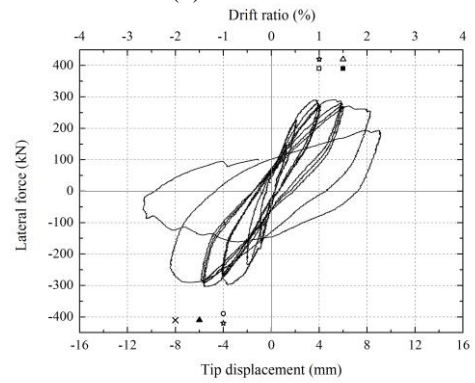
(c) 3-A-N1-M85



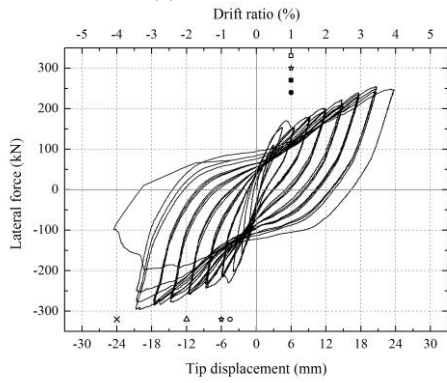
(d) 4-A-N2-M85



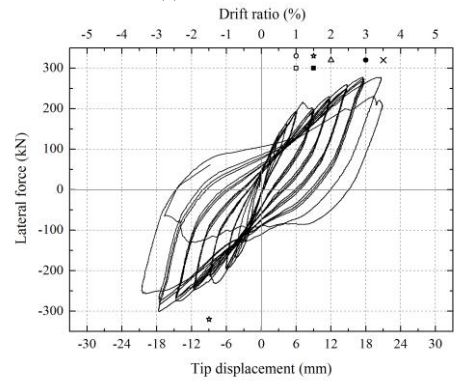
(e) 5-A-N1-M100



(f) 6-A-N2-M100



(g) 7-B-N2-M50



(h) 8-B-N2-M60

Continued-

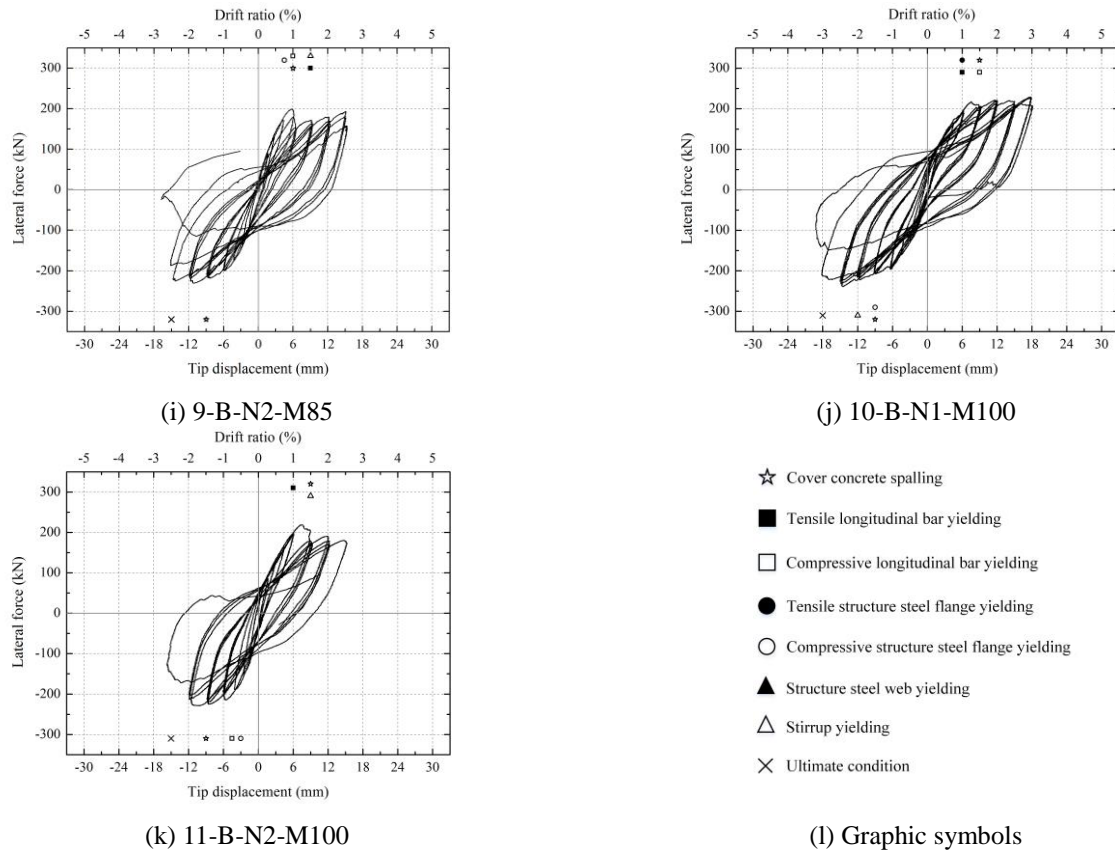


Fig. 4 Hysteresis curves of columns

3.1.3 Stirrup and structural steel web yielding, stirrup fractures or opening

The strain of the stirrups and structural steel web increased with increasing displacement amplitude. Before the yielding of transverse reinforcement and structural steel web, the columns developed stable hysteretic curves: the development of concrete cracks (particularly the width of the main diagonal cracks) was restrained. Partially confined concrete did not crush, obviously. After that, however, the damage to columns occurred more quickly, because of the rapid main diagonal crack development and core concrete crushing. Because the stirrups in columns were designed using the condition of flexural failure before shear failure, the shear force, crushed concrete dilating and longitudinal bars buckling together led to the stirrup fracturing or opening.

3.1.4 Loss of lateral load carrying capacity and failure mode

The short column specimens developed stable responses without significant strength degradation to drift ratios ranging from 1.5 to 2.5%, primarily depending on the axial load ratios and transverse reinforcement details (Fig. 4). Even though short columns behaved in a shear-dominant manner (inclined cracks caused by shear force) at drifts smaller than 1.5%, their failure exhibited shear-flexure failure characteristics. Failure occurred through the combination of concrete crushing, transverse hoop opening,

and longitudinal bar and structural steel buckling (Fig. 5). This is very different from the failure of the short column specimens tested by Jia *et al.* (2006), which exhibited shear failure mode. This occurred because (1) the shear capacity was designed to be larger than the flexural capacity; (2) shear capacity degradation was not significant, which was demonstrated by the fact that the largest width of inclined cracks for short columns was smaller than 2 mm, and the cracks did not seriously penetrate the core concrete (Fig. 5), because of the multiple stirrups and structural steel; (3) the crushing of concrete and buckling of longitudinal bars and structural steel led to the degradation of flexural strength in the cross-section. Therefore, the stirrups in the short columns not only restricted the inclined cracks, carrying a portion of the shear force, but also restricted the dilating of crushed concrete and buckling of longitudinal bars caused by the axial load and moment. Stirrup yielding was caused by the combination of shear force, axial load and moment.

The rational arrangement of stirrups and structural steel would confine the core concrete and restrict the inclined cracks, and would consequently change the brittle shear failure mode to a ductile shear-flexure failure mode.

3.2 Normal columns

The normal columns developed stable and plentiful hysteretic curves to drift ratios ranging from 2.0 to 3.5%. The initial yielding of steel, including structural steel and

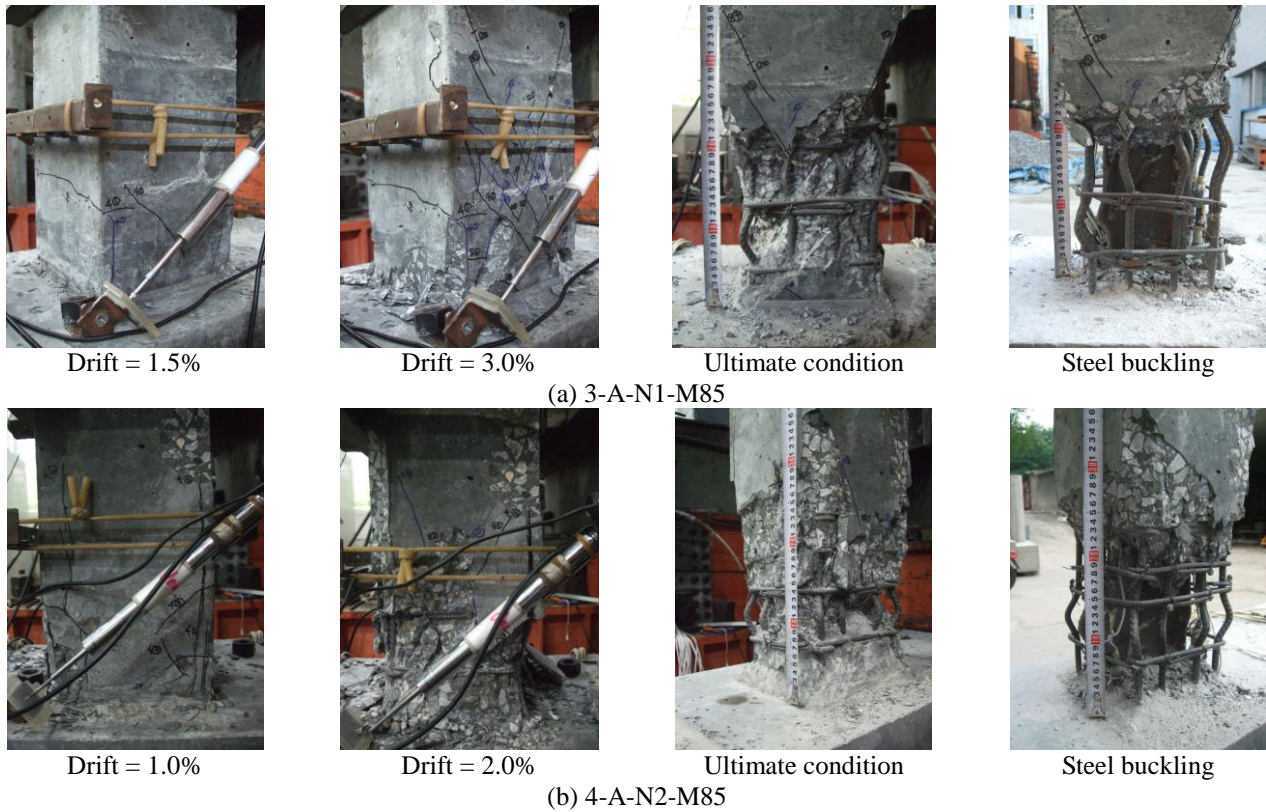


Fig. 5 Damage propagation at different steps and failure modes of short column specimens

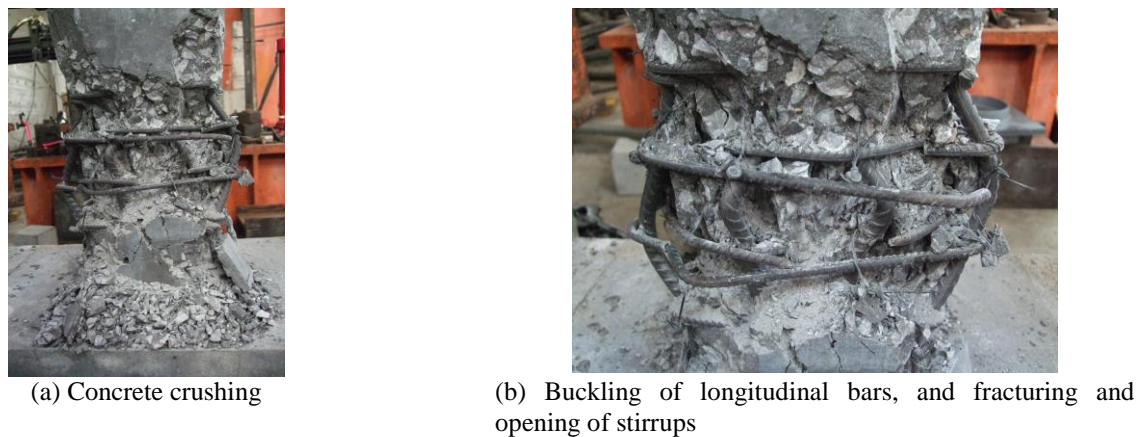


Fig. 6 Failure mode of normal column specimens (8-B-N2-M60)

longitudinal reinforcements happened at drift ratios ranging from 0.5 to 1.5%. Cover concrete spalling occurred at a drift ratio of 1.0 or 1.5%, which is later than the spalling time of short columns. After this point, cover concrete spalling diffused on column surfaces gradually, accompanying with longitudinal bar and structural steel buckling. During this process, only a few or no inclined cracks formed on the column surfaces parallel to the horizontal forces. Unlike for the short columns, all normal columns exhibited flexure failure characteristics (Fig. 6). The final stirrup fracturing or opening was resulted from crushed concrete dilating and longitudinal bar buckling, and caused that the columns could not bear the axial loads and lateral forces.

4. Length of critical region

The critical region length can be defined as the length of the member region that must be properly confined by transverse reinforcements such that the member could behave according to the prospective performance level (Pam and Ho 2009). The critical region should be effectively confined to achieve sufficient plastic rotation capacity and avoid brittle failure during inelastic deformation for SRHC normal columns. For SRHC short columns, the critical region should also be laterally confined to restrict the development of inclined cracks, besides to improve the flexural behavior. Then, brittle shear

failure mode was consequently changed to ductile shear-flexural failure mode.

The critical region length for each column specimen can be determined by physical observation (Pam and Ho 2009). Cover spalling was observed to occur during early inelastic drifts. The cracks on column surfaces increased in both number and width. However, in further inelastic drifts, major damages (including diagonal cracks; concrete core damage; longitudinal bar and structural steel yielding and buckling; and stirrup yielding, fracturing or opening) were concentrated within a limit height of the column near the stub footing. The extent of bar and structural steel yielding; and stirrup yielding, fracturing, or opening was found to be smaller than that of other types of damage. Therefore, it is proposed that the critical region length (L_p) is taken as the largest region suffering the following damage: (1) cover spalling penetrating the concrete core (L_c); (2) local buckling of longitudinal steel (L_{bl}); and (3) local buckling of structural steel (L_{bs}). For instance, Fig. 5 shows the observed critical region for two short column specimens. Based on the method of physical observation, the values of L_p , L_c , L_{bl} , and L_{bs} are summarized in Table 4. It is found from the table that: (1) L_c is larger than L_{bl} , because longitudinal bar buckling occurred only if the cover concrete had completely spalled off, and the stirrups and longitudinal bars were exposed; L_{bl} is typically larger than L_{bs} , because the structural steel is confined more strictly than the bars by concrete; (2) L_p is not obviously affected by stirrups; (3) in normal columns, L_p increases with compressive axial load; (4) in short columns, L_p approximately equals the column height. Based on the above, the critical region length L_p for SRHC columns is suggested as follows:

(1) For short columns, L_p is taken as the overall column height, regardless of the axial load level. That is, short columns should be confined by stirrups along the whole height.

(2) For normal columns, L_p is taken as 1.5 times the cross-sectional dimension if $n \leq 0.25$, and as 2.0 times the cross-sectional dimension if $0.25 < n \leq 0.38$.

5. Hysteretic behavior

5.1 Hysteretic curves and lateral load carrying capacity

The hysteretic curves shown in Fig. 4 trace the measured lateral force versus displacement response histories of both short and normal column specimens. Based on the curves, the measured peak lateral forces (F_p) and lateral forces at cover spalling (F_{sp}) for all specimens are listed in Table 4. Both F_p and F_{sp} were taken as the average values of the push and pull directions. As shown in Fig. 4 and Table 4, F_p varied significantly with different axial loads and stirrups. Because longitudinal bars and structural steel usually yielded at the drift of cover spalling point (Fig. 4); F_{sp} was close to or equal to F_p , but the former was more stable and the latter was more scattered depending on the axial load and stirrup characteristics; and columns might

suffer severe damage at peak force, lateral forces at cover spalling (F_{sp}) can be taken as the lateral load carrying capacity of SRHC short and normal columns.

5.2 Energy dissipation capacity and deformation capacity

The capacities of energy dissipation and deformation are important indicators of seismic performance of columns. The dissipated energy is evaluated as the areas surrounded by the hysteretic loops for each cycle. The cumulative dissipated energy is calculated by summing the energy dissipated in each cycle up to a certain displacement level. In particular, the total cumulative dissipated energy (E_{sum}) is defined by the energy dissipated during the test until failure (Légeron and Paultre 2000). The cumulative dissipated energy versus tip displacement (drift ratio) is plotted in Fig. 7. At the same time, the total cumulative dissipated energy for all columns is listed in Table 4.

The deformation capacity is quantified by the ultimate displacement ductility factor μ_Δ and the ultimate drift ratio θ_u . The ultimate displacement ductility factor μ_Δ is defined as the ratio of ultimate displacement (Δ_u) to yielding displacement (Δ_y) (Légeron and Paultre 2000). Δ_u is the post-peak displacement where the carrying capacity has declined to $0.8 F_{sp}$. And Δ_y is defined by the displacement which the lateral force F_{sp} would reach for a column stiffness equals to a secant stiffness of $0.75 F_{sp}$, because F_{sp} is taken as the lateral load carrying capacity of the SRHC short and normal columns. The ultimate drift ratio θ_u is taken as the ratio of the ultimate displacement to the height of the column. The trial values of Δ_y , Δ_u , μ_Δ and θ_u are also listed in Table 4. The following observations can be drawn from Table 4 and Fig. 7:

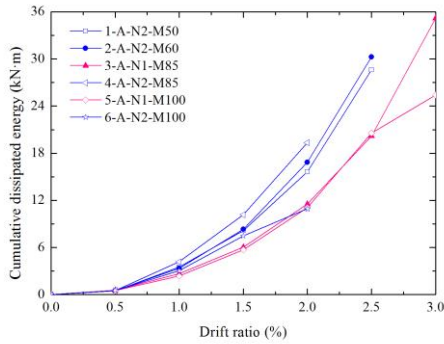
(1) The influence of the axial load level can be assessed through specimens with identical parameters but different axial load ratios, such as 3-A-N1-M85 and 4-A-N2-M85, or 5-A-N1-M100 and 6-A-N2-M100. Axial load is found to have a negative effect on energy dissipation and deformation capacity, which means that columns subjected to higher axial load levels exhibit diminished energy dissipation and deformation capacity, as shown in Table 4 and Fig. 7(a).

(2) By comparing 1-A-N2-M50, 2-A-N2-M60, 4-A-N2-M85, and 6-A-N2-M100, or 3-A-N1-M85 and 5-A-N1-M100, it can be found that although stirrups do not obviously affect the cumulative dissipated energy for a certain drift ratio, they significantly enhance the total cumulative dissipated energy (Fig. 7(a)), because stirrups significantly improve deformation capacity (Table 4). Both energy dissipation capacity and deformation capacity are approximately proportional to the effective confinement index of stirrups I_e (Paultre and Légeron 2001; Zhu *et al.* 2016), when other parameters are equal.

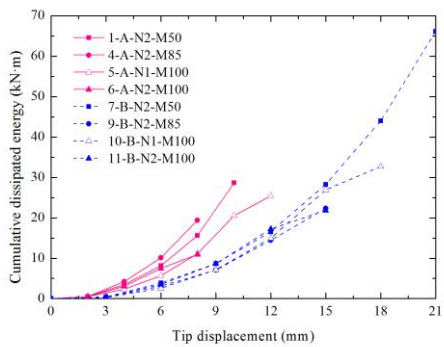
(3) The effect of shear span ratio can be assessed for four sets of columns (such as 1-A-N2-M50 and 7-B-N2-M50). In each set, the equivalent column for an SRHC short column with $\lambda = 2.0$ was a normal column with $\lambda = 3.0$. As shown in Fig. 7(b), under a certain tip displacement, the cumulative dissipated energy of short columns is obviously

larger compared to normal columns, which is mainly due to the higher lateral load resistance and more serious damage to the short column. However, from Table 4 and Fig. 7(b), it is found that the total cumulative dissipated energy of the short column is much smaller than that of normal columns, because the deformation capacity (μ_{Δ} and θ_u) of the former is much smaller. For example, the cumulative dissipated energy of 1-A-N2-M50 was larger than that of 7-B-N2-M50 for the same tip displacement smaller than 10 mm; however, the total cumulative dissipated energy of the former (28.6 kN•m) was much smaller than that of the latter (66.1 kN•m). At the same time, the decrease in energy dissipation and deformation capacity due to the decreasing shear span ratio is more serious for higher axial load levels. This can be found by comparing the values of E_{sum} , μ_{Δ} , and θ_u of 5-A-N1-M100, 6-A-N2-M100, 10-B-N1-M100, and 11-B-N2-M100 listed in Table 4. Therefore, the maximum axial load levels for short columns should be more strictly limited than that for normal columns. Meanwhile, it can be found that stronger stirrup confinement (i.e., larger I_c) is need for short columns than normal columns with the same axial load level to obtain similar energy dissipation and deformation capacities from Table 4.

(4) SRHC short columns confined by multiple stirrups may have good deformation capacity ($\mu_{\Delta} \geq 3.0$ and $\theta_u \geq 2.5\%$), despite the use of a relatively high axial load level ($n = 0.38$) and relatively small structural steel ratio ($\rho_{ss} = 3.58\%$).

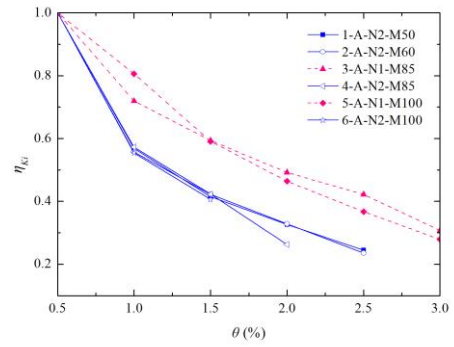


(a) Effects of axial load level and stirrup details

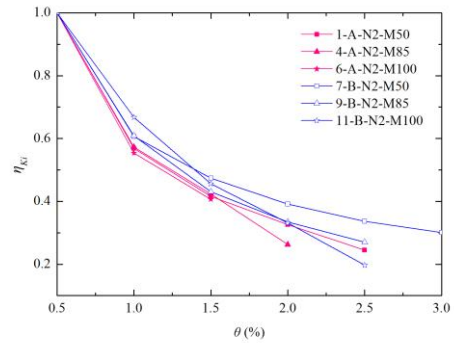


(b) Effect of shear span ratio

Fig. 7 Cumulative dissipated energy versus tip displacement for specimens

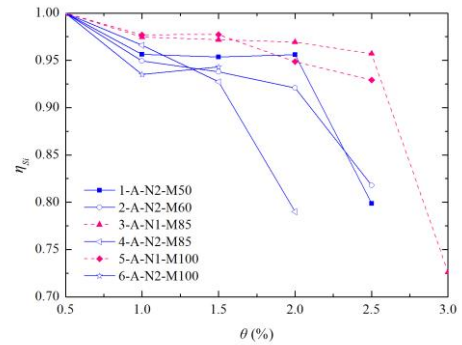


(a) Effects of axial load level and stirrup details

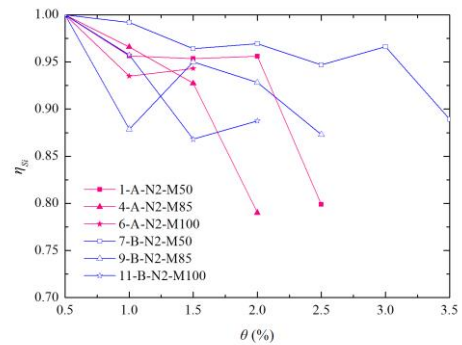


(b) Effect of shear span ratio

Fig. 8 Stiffness degradation of specimens



(a) Effects of axial load level and stirrup details



(b) Effect of shear span ratio

Fig. 9 Strength degradation of specimens

5.3 Stiffness degradation and strength degradation

The column stiffness at the i th drift level (K_i) can be measured by the averaged secant stiffness of the pull and push directions (Zhu *et al.* 2016). Because the SRHC columns behave elastic performance at the drift level of 0.5%, the former calculated stiffness is normalized by the stiffness at this drift (K_0): $\eta_{Ki} = K_i / K_0$. The values of K_0 of all columns are listed in Table 4. Fig. 8 presents the normalized stiffness at different drifts (η_{Ki}). So, the figure describes rigidity degradation with the increasing of drifts. Strength degradation at the i th drift level is described by a strength degradation factor (η_{Si}), which is expressed as the maximum lateral force in the last cycle divided by that in the first cycle at the i th drift: $\eta_{Si} = F_i^{3m} / F_i^{1m}$. Fig. 9 shows the variation in strength degradation with drift ratios. Based on the curves plotted in Figs. 8 and 9 and the data summarized in Table 4, it can be observed that:

(1) The normalized stiffness of short columns decreases gradually with increasing drift ratio. Strength degradation developed stably and gradually, and is not obvious ($\eta_{Ki} = 0.9-1.0$) before the last drift level. However, when specimens approach failure (during the last drift level), strength degradation occurs very abruptly. The above observations coincided with the failure process of SRHC short columns.

(2) By comparing 3-A-N1-M85 and 4-A-N2-M85, or 5-A-N1-M100 and 6-A-N2-M100, it is found that stiffness and strength degradation become faster in the short specimens subjected to higher axial load levels, as shown in Figs. 8(a) and 9(a). Similarly, it can be found from the two figures that stiffness and strength degradation is slower if the column is more strictly confined by stirrups (i.e., when I_e is larger).

(3) The effect of shear span ratio on stiffness and strength degradation can also be assessed for the four sets of columns mentioned in Section 5.2, such as 1-A-N2-M50 and 7-B-N2-M50. As shown in Figs. 8(b) and 9(b), stiffness and strength degradation is more rapid in SRHC columns with smaller shear span ratios. This occurs because damage to short columns (such as the formation of new inclined cracks, extension of old cracks) develops gradually during the stable cycling stage, while damage to normal columns is lower, except at the cover spalling drift level.

5.4 Shear displacement

The shear deformation of the region just 250 mm above the column end was measured by LVDTs. The region was the most damaged region along the columns. Fig. 10 shows the measured shear force-shear displacement relations of the region of several SRHC column specimens. For each specimen, the last portion of the curve just before failure was not plotted because the readings of the LVDTs were disturbed at that time. Fig. 11 also shows the contribution of shear displacement to the total displacement of the region at the peak displacement of each drift level. An analysis of the two figures leads to the following observations:

(1) The shear force-shear displacement curves of short columns with smaller axial load ratio (by comparing 5-A-

N1-M100 and 6-A-N2-M100) or stronger stirrup confinement (by comparing 1-A-N2-M50 and 6-A-N2-M100) are plumper. In all short column specimens, the percentage contribution of shear displacement which is about 30~40% of the total deformation, increases gradually with the development of drifts but does not change significantly. This is because the multiple stirrups and structural steel confined the concrete well (i.e., the shear capacity degradation was not significant), and avoided the shear failure of the specimens. The axial load and stirrups did not affect the percentage contribution of shear displacement obviously, because they did not change the failure mode of the short columns.

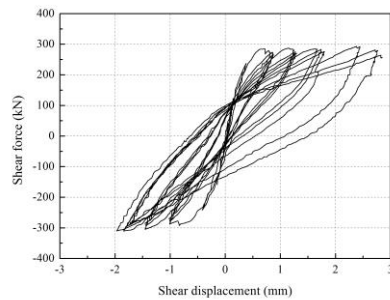
(2) The shear force-shear displacement curves of normal columns were plumper than those of short columns. At the same time, the percentage contribution of shear displacement of normal columns also increased gradually, but was always much smaller than that of short columns.

6. Conclusions

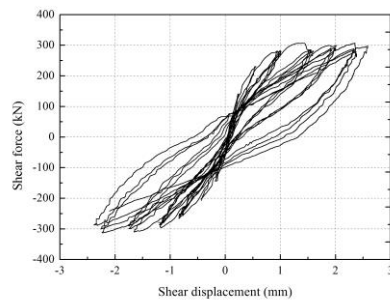
In this paper, the experimental results of a simulated earthquake loading test on six SRHC short columns and five SRHC normal columns were reported.

- SRHC short columns exhibited shear-flexure failure characteristics, because shear capacity was designed to be larger than flexural capacity, and because the shear capacity degradation was restricted by structural steel and multiple stirrups.
- The critical region length of SRHC short columns can be taken as the overall column height, regardless of axial load level. That is, short columns should be confined by stirrups along the whole height.
- Axial compression has a negative influence on the seismic performance of SRHC short columns. Columns subjected to larger compressive loads have weaker energy dissipation capacity and deformation capacity, and undergo faster stiffness degradation and strength degradation. In contrast, stirrups have a positive effect, and deformation capacity and energy dissipation capacity are both almost proportional to the effective confinement index of stirrups, when other parameters are equal.
- Shear span ratio significantly affects the seismic performance of SRHC columns. In comparison to SRHC normal columns, SRHC short columns exhibit more brittle failure modes, have weaker energy dissipation and deformation capacities, and undergo more rapid stiffness and strength degradation. The decrease in energy dissipation capacity and deformation capacity due to the decreasing of shear span ratio is more serious for larger axial load ratios. The maximum axial load levels for short columns should be more strictly limited than that for normal columns. Stronger stirrup confinement (i.e., larger I_e) is need for short columns than normal columns with the same axial load level to obtain similar energy dissipation capacity and deformation capacity. However, SRHC short columns confined by multiple stirrups may possess good seismic

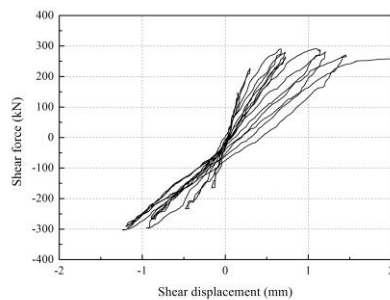
behavior with enough deformation capacity ($\mu_{\Delta} \geq 3.0$ and $\theta_u \geq 2.5\%$), even for relatively high axial load levels ($n = 0.38$) and relatively small structural steel ratios ($\rho_{ss} = 3.58\%$). SRHC short columns confined by multiple stirrups are suitable to be used in tall buildings in earthquake regions.



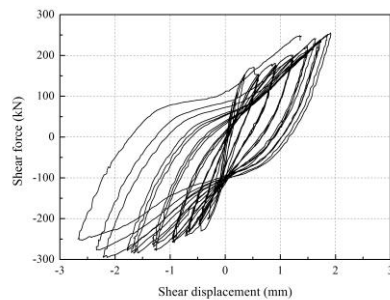
(a) 1-A-N2-M50



(b) 5-A-N1-M100



(c) 6-A-N2-M100



(d) 7-B-N2-M50

Fig. 10 Shear force-shear displacement relations

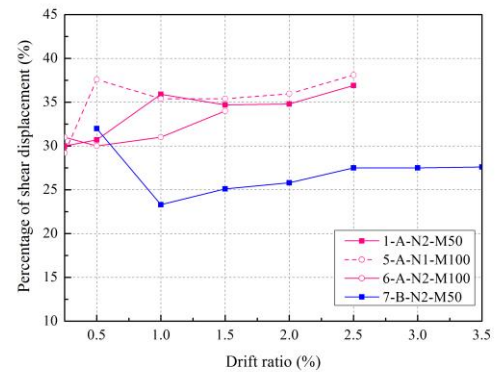


Fig. 11 Contribution of shear displacement to the total displacement

Acknowledgments

The financial assistance provided by the National Natural Science Foundation of China (Nos. 51508027 and 51178078), the China Postdoctoral Science Foundation (No. 2015M582587) and the Shaanxi Natural Science Foundation (No. 2016JQ5104) is gratefully acknowledged.

References

- Afroughsabet, V. and Ozbakkaloglu, T. (2015), "Mechanical and durability properties of high-strength concrete containing steel and polypropylene fibers", *Constr. Build. Mater.*, **94**(7), 73-82.
- Bai, Z.Z. and Au, F.T.K. (2013), "Flexural ductility design of high-strength concrete columns", *Struct. Des. Tall Spec. Build.*, **22**(1), 92-115.
- Chen, C.C. and Lin, N.J. (2006), "Analytical model for predicting axial capacity and behavior of concrete encased steel composite stub columns", *J. Constr. Steel Res.*, **62**(5), 424-433.
- Chen, Z.P., Xu, J.J., Chen, Y.L. and Xue, J.Y. (2016), "Axial compression ratio limit values for steel reinforced concrete (SRC) special shaped columns", *Steel Compos. Struct.*, **20**(2), 295-316.
- El-Tawil, S. and Deierlein, G.G. (1999), "Strength and ductility of concrete encased composite columns", *J. Struct. Eng.*, **125**(9), 1009-1019.
- Ellobody, E. and Young, B. (2011), "Numerical simulation of concrete encased steel composite columns", *J. Constr. Steel Res.*, **67**(2), 211-222.
- Fang, L., Zhang, B., Jin, G.F., Li, K.W. and Wang, Z.L. (2015), "Seismic behavior of concrete-encased steel cross-shaped columns", *J. Constr. Steel Res.*, **109**(6), 24-33.
- Hadi, M.N.S. (2005), "Behaviour of high strength axially loaded concrete columns confined with helices", *Constr. Build. Mater.*, **19**(2), 135-140.
- Hassan, W.M., Hodhod, O.A., Hilal, M.S. and Bahnasaway, H.H. (2017), "Behavior of eccentrically loaded high strength concrete columns jacketed with FRP laminates". *Constr. Build. Mater.*, **138**(5), 508-527.
- Ho, J.C.M., Lam, J.Y.K. and Kwan, A.K.H. (2010), "Effectiveness of adding confinement for ductility improvement of high-strength concrete columns", *Eng. Struct.*, **32**(3), 714-725.
- Hong, K.N., Han, S.H. and Yi, S.T. (2006), "High-strength concrete columns confined by low-volumetric-ratio lateral ties", *Eng. Struct.*, **28**(9), 1346-1353.

- JGJ138 (2001), Technical specification for steel reinforced concrete composite structures, China Ministry of Construction, Beijing, China.
- Jia, J.Q., Jiang, R. and Hou, T. (2006), "Experimental study on the seismic performance of steel reinforced super high-strength concrete columns", *China Civ. Eng. J.*, **39**(8), 14-18.
- Lam, J.Y.K., Ho, J.C.M. and Kwan, A.K.H. (2009), "Flexural ductility of high-strength concrete columns with minimal confinement", *Mater. Struct.*, **42**(7), 909-921.
- Légeron, F. and Paultre, P. (2000), "Behavior of high-strength concrete columns under cyclic flexure and constant axial load", *ACI Struct. J.*, **97**(4), 591-601.
- Ma, H., Xue, J.Y., Liu, Y.H. and Dong, J. (2016), "Numerical analysis and horizontal bearing capacity of steel reinforced recycled concrete columns", *Steel Compos. Struct.*, **22**(4), 797-820.
- Ma, H., Xue, J.Y., Zhang, X.C. and Luo, D. (2013), "Seismic performance of steel-reinforced recycled concrete columns under low cyclic loads", *Constr. Build. Mater.*, **48**(11), 229-237.
- Moretti, M.L. and Tassios, T.P. (2006), "Behavior and ductility of reinforced concrete short columns using global truss model", *ACI Struct. J.*, **103**(3), 319-327.
- Moretti, M.L. and Tassios, T.P. (2007), "Behavior of short columns subjected to cyclic shear displacement: Experimental results", *Eng. Struct.*, **29**(8), 2018-2029.
- Naito, H., Akiyama, M. and Suzuki, M. (2011), "Ductility evaluation of concrete-encased steel bridge piers subjected to lateral cyclic loading", *J. Bridge Eng.*, **16**(1), 72-81.
- Pam, H.J. and Ho, J.C.M. (2009), "Length of critical region for confinement steel in limited ductility high-strength reinforced concrete columns", *Eng. Struct.*, **31**(12), 2896-2908.
- Paultre, P., Légeron, F., and Mongeau, D. (2001), "Influence of concrete strength and transverse reinforcement yield strength on behavior of high-strength concrete columns", *ACI Struct. J.*, **98**(4), 490-501.
- Pham, T.M. and Hadi, M.N.S. (2014), "Confinement model for FRP confined normal- and high-strength concrete circular columns", *Constr. Build. Mater.*, **69**(10), 83-90.
- Wang, D.Y., Wang, Z.Y., Smith, S.T. and Yu, T. (2017), "Seismic performance of CFRP-confined circular high-strength concrete columns with high axial compression ratio", *Constr. Build. Mater.*, **134**(3), 91-103.
- Wang, Y.B. and Liew, J.Y.R. (2016), "Constitutive model for confined ultra-high strength concrete in steel tube", *Constr. Build. Mater.*, **126**(11), 812-822.
- Xiao, J.Z. and Zhang, C. (2006), "Experimental investigation on the limitation of axial load level of RC columns in seismic regions", *Adv. Struct. Eng.*, **9**(3), 349-359.
- Xue, J., Chen, Z.P., Zhao, H.T., Gao, L. and Liu, Z.Q. (2012), "Shear mechanism and bearing capacity calculation on steel reinforced concrete special-shaped columns", *Steel Compos. Struct.*, **13**(5), 473-487.
- Zheng, S.S., Zhang, L., Li, L., Hu, Y. and Hu, C.M. (2012), "Experimental research on seismic behavior of steel reinforced high strength concrete frame columns", *J. Build. Struct.*, **33**(5), 124-132.
- Zhu, W.Q., Jia, J.Q., Gao, J.C. and Zhang, F.S. (2016), "Experimental study on steel reinforced high-strength concrete columns under cyclic lateral force and constant axial load", *Eng. Struct.*, **125**(10), 191-204.
- Zhu, W.Q., Meng, G. and Jia, J.Q. (2014), "Experimental studies on axial load performance of high-strength concrete short columns", *Proc. ICE: Struct. Build.*, **167**(9), 509-519.